Plasmon Induced Nano Au Particle Decorated over S,N-Modified TiO2 for Exceptional Photocatalytic Hydrogen Evolution under Visible Light

ARTICLE *in* ACS APPLIED MATERIALS & INTERFACES · DECEMBER 2013

Impact Factor: 6.72 · DOI: 10.1021/am403865r · Source: PubMed

4 AUTHORS:

Soumyashree Pany
Institute of Minerals and Materials Technol…
5 PUBLICATIONS **71** CITATIONS
SEE PROFILE

Brundabana Naik
Korea Advanced Institute of Science and Te…
24 PUBLICATIONS **398** CITATIONS
SEE PROFILE

Satyabadi Martha
Institute of Minerals and Materials Technol…
31 PUBLICATIONS **573** CITATIONS
SEE PROFILE

Kulamani Parida
ITER, Siksha 'O' Anusandhan University
346 PUBLICATIONS **6,819** CITATIONS
SEE PROFILE

RSC Advances

RSC Publishing

PAPER

View Article Online
View Journal | View Issue

Facile fabrication of mesoporosity driven N–TiO_2@CS nanocomposites with enhanced visible light photocatalytic activity†

Cite this: *RSC Advances*, 2013, **3**, 4976

Soumyashree Pany, K.M. Parida* and Brundabana Naik

For the efficient utilization of visible light from solar light illumination, wormhole mesoporous N-doped TiO_2 modified with carbon and sulfur (abbreviated as N–TiO_2@CS nanocomposites) have been fabricated using a sol–gel auto-combustion method. The prepared samples under different calcination temperatures were thoroughly characterized by XRD, TEM, FTIR, BET Surface area, UV-Vis DRS, XPS and PL. It has been demonstrated that in N–TiO_2@CS nanocomposites, incorporated N in the crystal lattice of TiO_2 exist as N–Ti–O, sulfur exist as sulfate ions (S^{6+}) on the TiO_2 surface and carbon species were modified on the surface of the photocatalyst. *N*-doping narrows the band gap and sulfate species on the surface of TiO_2 act as co-catalyst. Moreover, the presence of surface carbon species enhances visible light harvesting and stimulates to separate photo generated charge carriers, which makes the system more potential towards photocatalytic application. The photocatalytic activities of the as prepared catalyst were evaluated for phenol degradation under visible light irradiation. The higher photocatalytic activity of the N–TiO_2@CS nanocomposite calcined at 400 °C (STU400) is attributed to the synergistic combination of C, N and S atoms, the wormhole mesoporous frame with high surface area and high crystalline anatase phase of TiO_2. The overall photocatalytic activity and the proposed mechanism are further confirmed through PL spectra and trapping of hydroxyl radicals.

Received 5th November 2012,
Accepted 15th January 2013

DOI: 10.1039/c3ra22775h

www.rsc.org/advances

1 Introduction

Researchers have paid much attention towards the development of valuable products by adopting sustainable methods, that is, green chemistry. It has been seen for the last several years that utilization of direct solar light is becoming a more greener approach for an energy solution (photocatalytic water splitting for clean H_2 fuel) as well as environmental clean-up (photocatalytic degradation of pollutants). Therefore, the development and design of a visible light active photocatalyst for direct sun light harvesting has drawn broad interdisciplinary attention and much research fascination.

Among all oxide semiconductor photocatalysts, titanium dioxide (TiO_2) exhibits excellent photocatalytic activity and is used in a wide range of applications.[1–4] However, a high charge recombination factor and a large band gap in TiO_2 restricts its photocatalytic application.[5,6] Therefore, the challenge in the field of photocatalysis is to make new materials which could effectively use the maximum part of solar light, inhibit the electron-hole recombination rate and improve the photocatalytic activity of TiO_2. Various metal ions doped in TiO_2 have been reported by many researchers, however there is only limited success due to photo-corrosion and increasing numbers of recombination centers.[7] However, an effective way to narrow the band gap of TiO_2 is through non metal doping such as N, C, S, P, B and F. [8–13] Until today, significant achievements have been gained from N doping (TiO_2), which decreases the band gap by either the mixing of nitrogen 2p states with oxygen 2p states on the top of the valence band or a creation of an N induced mid gap level and shifting the optical response towards the visible region.[14–16] In contrast, the incorporation of carbon into TiO_2 can also extend the optical response towards the visible region. It is well reported that in the carbon modified TiO_2, the carbon species leads the major role towards the absorption of visible light where it acts as a surface sensitizer.[17] Wang *et al.* also demonstrated that the presence of nano sized carbon species on the catalyst surface trap photoexcited electrons from the conduction band to promote the separation of charge carriers and generate a hetero type structure which sensitizes TiO_2.[18] Recently, Xu *et al.* synthesized hydrothermally N-doped TiO_2/C nanocomposites and provided strong evidence for the promotion of the separation of charge carriers and for keeping them highly reactive towards the photocatalytic activity under visible light irradiation. This is due to direct optical charge transfer

Colloids and Materials Chemistry Department, Institute of Minerals and Materials Technology (CSIR), Bhubaneswar - 751 013, Orissa, India.
E-mail: paridakulamani@yahoo.com; Fax: +91-674-2581637; Tel: +91-674-2379425
† Electronic supplementary information (ESI) available. See DOI: 10.1039/c3ra22775h

transition between N–TiO_2 and the carbon species.[19] In recent days, these new thoughts received much attention and opened a new area in the field of photocatalysts. Depending upon the synthetic conditions and the type of precursor used in the reaction process, more than one oxidation state [S^{2-}, S^{+4}, S^{+6}] is observed for the sulfur ion.[20,21] The cationic S-doped titania reported by Ohno *et al.* were found to have better visible light absorption and photocatalytic activities in comparison to the anionic S-doped titania.[22] Our group has also studied the photocatalytic activity of sulphate modified titania under visible light irradiation.[23–26]

However, recent emphasis has been on the combination of cation and anion or anions together within the crystal lattice of TiO_2, in which dramatic enhancement of photocatalytic activity has been reported.[27] Many groups have synthesized N,C–TiO_2[28,29], N,S–TiO_2[30–32], C,S–TiO_2[33], and N–C–S modified TiO_2[34] by using different preparation methods and evaluate their photocatalytic activity. However until today, there has been no report on the combination of both anions (N, C) and a cation (S) incorporated in TiO_2, which forms a hetero type structure and mainly responsible for inhibiting the recombination of charge carriers.

In the present study, mesoporous N–TiO_2@CS nanocomposites have been prepared by a sol–gel auto-combustion method which possesses several positive aspects, such as nano crystalline anatase phase, visible light absorption and high surface area with wormhole mesoporous architecture. The most reasonable factor in the N–TiO_2@CS nanocomposite is the incorporation of nitrogen in to the crystal lattice of TiO_2 and the presence of carbon and sulfate species on the catalyst surface. These surface species avoid recombination of charge carriers by taking the photogenerated electron from the conduction band and makes it more potential towards higher photocatalytic activity. The photocatalytic activities of the as prepared catalyst has been tested for phenol degradation under visible light irradiation and investigated the formation and role of most reactive oxygen species ($^{\cdot}OH$) over N–TiO_2@CS nanocomposite.

2. Experimental

2.1 Preparation of photocatalysts

The hydrate of titanium oxysulfate sulfuric acid complex ($TiOSO_4 \times H_2SO_4 \times H_2O$) (Sigma Aldrich), sucrose (Merck), and urea (Merck) are used as such without further purification. Wormhole mesoporous N–TiO_2@CS nanocomposites were prepared by adopting a sol–gel-auto combustion method using $TiOSO_4$ as precursors for both titania and sulfur. In this process, we employed sucrose as a templating agent and C source where urea acts as both the N dopant source as well as fuel. The weight ratio of sucrose/$TiOSO_4$/water was maintained, 1 : 1 : 85 in solution. In a typical procedure 17.1 g of sucrose was dissolved in 153 ml distilled water and the mixture was stirred for about 45 min, then 13.8 g of $TiOSO_4$ was added and after 2 h of stirring, 9 g of urea was added to it. The stirred mixture solution was heated at 100 °C in open air until it turned to dry gel, which on further heating automatically ignited as a result of a thermally induced oxidation reduction reaction. Finally, after auto-ignition, a dry gel is formed and calcined at temperatures in the range 400 to 800 °C. The as prepared samples are labeled as STU-*T*, where *T* denotes the calcination temperature such as STU400 and STU500. For comparison purpose, TiO_2@CS and N–TiO_2@S were prepared by taking sucrose and urea, respectively. In the combustion process, thermal decomposition of urea generates NH_3, which act as nitrogen source as well as creating reducing atmosphere. The same concept has been adopted by many researchers and prepared N doped TiO_2.[8] In our preparation method thermal decomposition of urea successfully follow up the above statements and suggests the carbon dopant source arises from the sucrose not from the urea.

2.2 Characterizations

The X-ray powder diffraction (XRD) pattern was performed on Philips 1710, X-ray diffractometer with Cu-Kα radiation and the patterns were recorded between 10° and 80° with a step 0.05° s^{-1}. A UV-Vis Spectrometer (Varian Cary 100) was used to record diffuse reflectance spectra in the range 200–800 nm using boric acid as the standard. Surface morphologies as well as their relationship to each other on the atomic scale were observed through a transmission electron microscope (TEM) (FEI, TECNAI G^2, TWIN) operating at 200 kV. The samples for electron microscopy were prepared by dispersing the powder in ethanol and coating a very dilute suspension on carbon-coated Cu grids. TEM images were recorded by using a Gatan CCD camera. The X-ray photoelectronic spectroscopy was performed with Kratos Axis 165 with a dual anode (Mg and Al) apparatus using the Mg-Kα source. Charge neutralization of 2 eV was used to balance the charge of the sample. Binding energies of the samples were reproducible within $\pm$0.1 eV. By using ASAP-2020, N_2 adsorption-desorption isotherm were measured at 77 K from which the surface area (BET method), the pore size (BJH model) and pore volume (V_P) are calculated. Photoluminescence (PL) studies were carried out with Fluorescence spectrometer FLUOROMAX-4.

2.3 Photocatalytic reaction procedure

The photocatalytic decomposition of phenol was performed using a quartz reactor with a water circulation facility at the outer wall of the reactor and with a specific outlet for the sample collection. For the evaluation of the photocatalytic activity, photocatalytic phenol degradation was carried out by taking 100 mg catalyst in an aqueous solution of phenol (10^{-4} M, 40 mL). The photocatalytic experiment was carried out under solar light for 180 min. Prior to the start of the light experiment, a dark adsorption experiment was carried out for 1 h under continuous stirring condition. The samples were centrifuged and filtered through regular time intervals. The cleared residual phenol concentration was analyzed by Varian Cary UV-Vis spectrophotometer. Before spectrophotometric analysis, the color was developed by addition of 2.5 ml of 0.5 M ammonium hydroxide solution followed by phosphate buffer to maintain the pH in the range 7.7–7.9. After the pH adjustment, 1 ml of 4-aminoantipyrene (Merck, 98%) and 1

ml of potassium ferricyanide (Aldrich, 99.5%) was added in order to develop red color. Then it was analyzed with UV-Vis Spectrometer (Varian Cary 100) at 504 nm. All photocatalytic experiments in this investigation were observed with no more than 3% deviation when repeated. Intensity of solar light was measured using a Digital Illuminance Meter (TES-1332A, Taiwan). The sensor was always set in the position of maximum intensity and solar light intensity was measured for every hour between 10:00 and 14:00 h. The average light intensity was around 100 000 lx, which was nearly constant during the experiments.

2.4 Determination of ˙OH radicals

The formation of ˙OH on the sample surface under visible light irradiation was analyzed through a fluorescence technique using terephthalic acid which readily reacts with ˙OH to produce highly fluorescent product 2-hydroxy terephthalic acid. The PL intensity of 2-hydroxy terephthalic acid is proportional to the amount of ˙OH. In a typical experimental procedure, 200 mg of the as-prepared catalyst was added to 5 $\times$ 10^{-4} M terephthalic acid solution with a concentration of 2 $\times$ 10^{-3} M NaOH. The PL spectrum of 2-hydroxy-terephthalic acid was measured on a fluorescence spectrophotometer FLUOROMAX-4. After visible light irradiation, the reaction solution was centrifuged and the filtrate part was taken to measure the PL spectra. The 2-hydroxy-terephthalic acid solution gave peak intensity at 426 nm by the excitation of wavelength at 315 nm.

3 Results and discussion

3.1 Structural characterization

To determine the phase structure, powdered XRD study has been carried out. Fig. 1 represents the XRD patterns of N–TiO_2@CS nanocomposites calcined at various temperatures. The XRD patterns are identical with the standard pattern of anatase phase (JCPDS-21-1272). From Fig. 1, it is clearly observed that the sample calcined at 400 °C shows a broad peak around 25.4° corresponding to the (101) plane diffraction of anatase TiO_2. The crystallite sizes of all the as-prepared nanocomposites were calculated by using the Scherrer formula (eqn (1)) and are listed in Table 1.

$$D = K\lambda/\beta\cos\theta \quad (1)$$

Where λ is the wavelength of Cu-Kα used and β is the full width at half-maximum of the diffraction peak, K is a shape factor (0.94) and θ is the angle of diffraction. The XRD pattern shows that both STU400 and STU500 exhibit only anatase phase with small crystallite size. As N, C and S species are incorporated into TiO_2, these species have a significant role to inhibit the phase transformation as well as controlling the crystallite size. The sample calcined at 400 °C has a crystallite size of 13.16 nm, however a slight increase in crystallite size at 500 °C (14.08 nm) suggests the stabilization of the anatase phase as well as maintaining low crystallite size, which is well consistent with our earlier study.[26] This is because the slightly short O–O atomic bond length of the sulfate tetrahedral (which varies in between 0.238 and 0.243 nm) in comparison to the O–O atomic bond length of anatase (0.245 and 0.304 nm) is well favored to be anchored to the anatase phase of the TiO_2 crystal in contrast to rutile and brookite phases. [35] So anatase is the most probable phase for fixing sulfate ions to its surface. The interactions of SO_4^{2-} with the TiO_2 network also hinder the phase transfer and growth of the particle.[36] A similar observation has also been observed in the case of PO_4^{3-} incorporated titania.[11] At higher calcined temperatures the phase transformation of anatase to rutile and increase in crystallite size suggest a loss of sulfate species from the surface of TiO_2. It has been well reported that the anatase phase of TiO_2 shows better photocatalytic activity than the rutile phase.[37] As the sample calcined at 400 °C shows only anatase phase and low crystallite size it might be one of the possible reasons suggested for higher photocatalytic activity. There are also other potential factors responsible for higher photocatalytic activities which are discussed later.

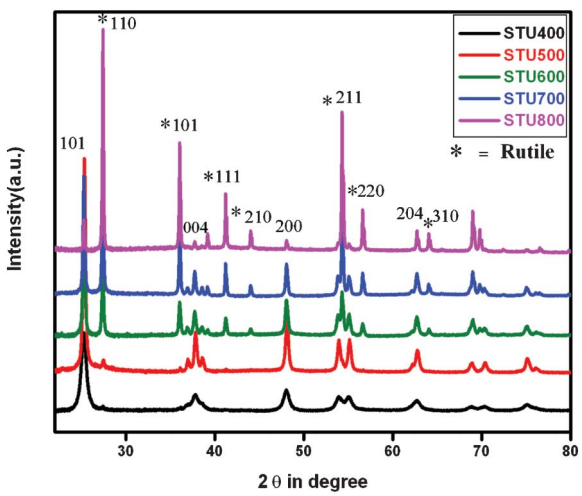

Fig. 1 X-ray diffraction patterns of STU nanocomposites calcined at various temperatures.

TEM analysis has been performed to examine the particle morphology. Fig. 2(a) represents the TEM image of the STU400 nanocomposite. From the figure, a disordered wormhole like structure was observed. It may be due to the intergrowth of primary particles with the rough and uneven surface which leads to aggregates with significant extra frame work void space. The observed morphology is well consistent with N_2 sorption isotherms which will be discussed in the next section. The selected area electron diffraction (SAED) patterns (Fig. 2b) taken from the nano crystalline particles confirm both the crystalline nature as well as the anatase phase of TiO_2. The highly intense concentric diffraction ring observed in the SAED pattern again confirms that the (101) plane of anatase is highly dominating on the surface. It is well consistent with the XRD data. It is expected that combination of high crystallinity with small particle size helps with the faster diffusion of charge carriers to the surface without recombination and enhances the light harvesting properties.[8] In addition to the above, the wormhole mesoporous frame between the nano-

Table 1 Crystallite size, BET surface area, pore size, pore volume and band gap of STU photocatalysts

Sample code	Crystallite size (nm)	BET surface area ($m^2\ g^{-1}$)	Pore size (Å)	Pore volume ($cm^3\ g^{-1}$)	Band gap (eV)
STU400	13.16	72	76	0.13	2.7
STU500	14.08	21	172	0.09	2.9
STU600	30.78	6	214	0.03	3.0
STU700	72.35	–	–	–	3.0
STU800	76.15	–	–	–	3.1

particles also plays an important role for light harvesting as the porous frame allows light to scatter inside the porous channels and effectively enhances the light absorption capacity.[38] Indeed, the mesoporous nature of the material reduces the diffusion length of charge carriers to a few nanometers and provides an easy route for the diffusion of reactants due to fewer diffusion barriers. The EDX spectrum (Fig. 2c) was taken at several random spots on the specimen and all the spectra reveal that N, C, S, O and Ti are well distributed on TiO_2.

3.2 Surface area

The specific surface area and textural properties of mesoporous N–TiO_2@CS nanocomposites have been studied using BET method by N_2 adsorption-desorption isotherms at 77 K. Table 1 shows the physicochemical properties of N–TiO_2@CS nanocomposites. Fig. 3 shows a nitrogen sorption isotherm and the inset figure represents the pore size distribution curve of N–TiO_2@CS nanocomposites calcined at 400 and 500 °C (STU400 and STU500). From the isotherm curve it reveals that both the curves display a type IV isotherm, characteristic of mesoporous materials. It shows an H2 hysteresis loop which can be observed in the pores with narrow necks and wider bodies (ink bottle pores). However, here the mesoporosity is not as for typical mesoporous materials like MCM-41 and SBA-15.[39] Here, aggregation of smaller particles creates the inter particle wormhole mesoporosity. The STU-400 photocatalyst displays a surface area of 72 $m^2\ g^{-1}$ but as the calcination temperature increases to 500 °C, a drastic decrease in the surface area value from 72 $m^2\ g^{-1}$ to 21 $m^2\ g^{-1}$ suggests destruction of wormhole mesoporosity due to inter growth of crystallite size. Furthermore, the highest specific surface area of STU400 might be due to the presence of the sulfate ion which has a great impact on enhancing the surface area. It is well reported by our groups that modification by sulfate ions increases the surface area to a great extent and it works better when it is dispersed into the mesoporous frame.[26] Hence for this reason, STU400 shows the highest photocatalytic activity, which is discussed later. The inset in Fig. 3 represents the pore size distribution curve of STU400 and STU500 which is calculated by using the BJH equation from the desorption isotherm. From the inset in Fig. 3, a narrow intense pore size distribution with average pore diameter between 20–60 Å is observed for the sample calcined at 400 °C (STU400). On further increase of calcination temperature a remarkable shifting towards the right suggests an increase in pore size and another possible cause might be due to aggregation of the greater crystallite size.[40] Among all the as-prepared STU photocatalysts, STU400 shows the highest surface area with a pore volume of 0.13 $cm^3\ g^{-1}$ which may be due to the well developed mesoporosity. The high BET surface area suggests abundant surface reactant sites for adsorption of reactant

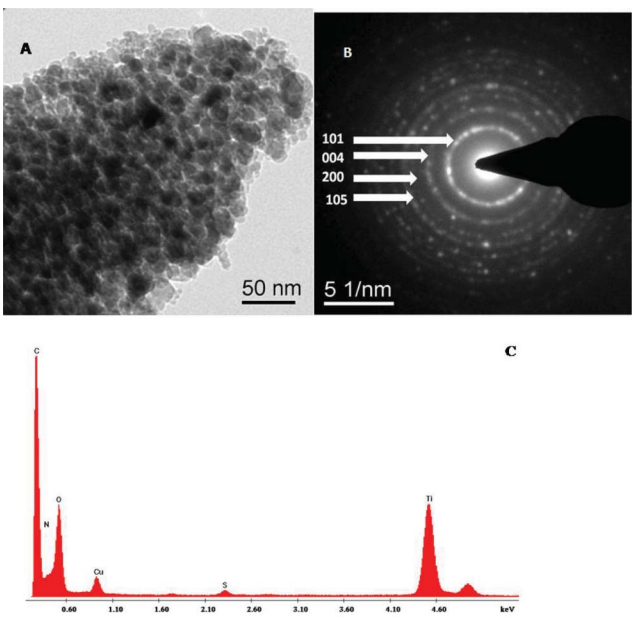

Fig. 2 TEM image of STU400 composites exhibiting wormholes and (b) corresponding selected area diffraction pattern and (c) EDX spectrum from an arbitrary region showing the presence of N, C, S in the sample.

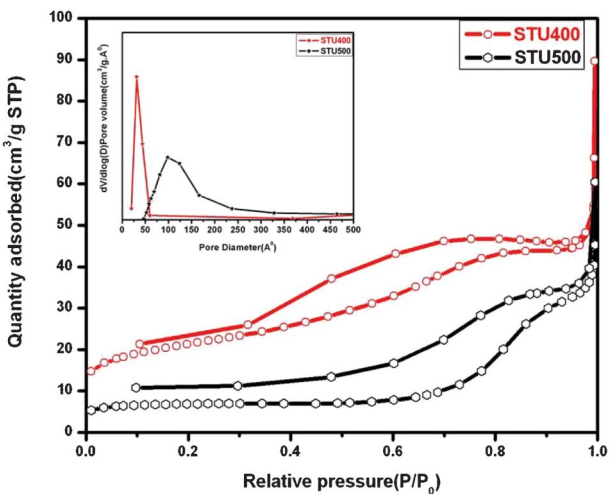

Fig. 3 N_2 adsorption desorption isotherm of STU400 and STU500.

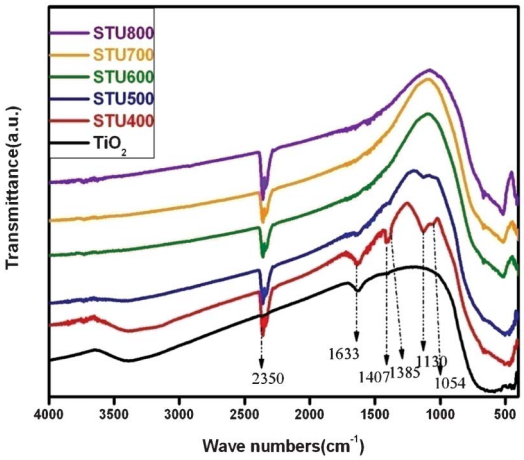

Fig. 4 FTIR spectra of STU nanocomposites.

molecule and the wormhole mesoporous frame is potentially important for photocatalysis due to channel branching within the frame which enhances light harvesting and decreases the diffusion length of charge carriers.

3.3 Spectroscopic investigations

The bonding characteristic of functional groups in the as-prepared N–TiO_2@CS nanocomposites has been identified by using FTIR spectroscopy. From Fig. 4, a broad peak in the region 3000–3600 cm^{-1} is assigned to the stretching vibration mode of adsorbed water and another peak observed at 1633 cm^{-1} is assigned to the bending vibration of surface hydroxyl groups. It is well known that adsorbed water and hydroxyl groups influence the photocatalytic activity.[26,30] A characteristic intense peak around 2350 cm^{-1} is assigned to the C=O stretching for atmospheric CO_2.[41] Furthermore, a doublet peak around 1407 and 1385 cm^{-1} suggests the existence of carbonate and hyponitrite groups.[19,41] The peak corresponding to 1054 and 1130 cm^{-1} is due to the presence of the sulfate group from precursors.[26,30] At a lower frequency region at around 500 cm^{-1}, the peak is due to the anatase phase of TiO_2.[41]

To study the optical response of N–TiO_2@CS nanocomposites, their UV visible absorption spectra were measured. Fig. 5 depicts a comparison study of optical absorbance of the as prepared STU catalyst calcined at various temperatures with neat TiO_2. The band gap of the entire as prepared sample calcined at different temperatures is listed in Table 1. As shown in the figure, remarkable red shifts, having a band gap of 2.7 and 2.9 eV, are observed for STU400 and STU500. The inset in Fig. 5 represents the optical absorbance of STU400, which shows absorption of visible light towards the red end with a band gap of 2.7 eV. The remarkable red shift may be assigned to the existence of N, C and S species in the N–TiO_2@CS nanocomposites. This is also further supported by the mixing of the N 2p with the O 2p state of TiO_2 and sulfate, which may form a localized state just above the valence band of TiO_2 and narrow the energy gap.[14,16,30,42] Moreover, not only N and S incorporation but also surface modified carbon enhances visible light absorption and reduces reflection of light.[17–19] The stronger absorption for the sample STU400 may be assigned to a synergistic effect of nitrogen, carbon and sulfur, which will be further confirmed from XPS. With the rise in calcination temperature, the increase in blue shift of the absorbance band suggests losses of N, C and S from the N–TiO_2@CS nanocomposites. The visible light absorbance of N–TiO_2@CS has great importance in the practical purpose because it can be activated by solar light.

Fig. 6 depicts XPS spectra for (a) N 1s (b) C 1s (c) S 2p core levels of N–TiO_2@CS nanocomposites calcined at 400 °C (STU400). Three deconvoluted peaks were observed at *ca.* 399.7, 400.1 and 401.1 eV for the N–TiO_2@CS nanocomposite. The peak appearing around 399.7 eV is attributed to anionic N^- in the O–Ti–N linkage.[19,43] The substitutional doping is more effective and responsible for absorbing visible light by reducing the band gap by 0.13 eV on creating a localized state above the valence band.[16] The N 1s binding energy appearing at 400.1 and at 401.1 eV may be due to oxidized N such as the O–N–Ti linkage or some surface oxidation.[44] The oxidized O–N–Ti environment also has some important role in the photocatalytic activity.[45] The atomic content of N in STU400 was calculated from XPS and found to be 1.7 atom%.

Deconvolution of the C 1s spectrum affords three components at 284.8, 286.3 and at 288.9 eV shown in Fig. 6(b). The main C 1s peak corresponds to 284.8 generally assigned to adventitious elemental carbon. The peak at 286.3 and at 288.9 eV can be ascribed to oxygen bound species such as C–O and C=O respectively.[17,19,46] No C1s peak observed at 281 eV confirms that carbon does not substitute oxygen atom in the lattice of anatase TiO_2.[18,19] Therefore, here carbon species are present on the surface of the catalyst and form nanocomposite material. It has been well reported that surface adsorbed carbonate links with TiO_2 as Ti–O–C and Ti–O–C–O bonds.[17–19] The formation of intimate contact between surface adsorbed carbon species and N,S incorporated TiO_2 favors charge transfer of photoexcited electrons and gave it more potential towards higher visible light photocatalysis.[17–19] The surface carbon species not only absorbs visible light at a longer wavelength but enhances the reactivity of photogenerated charge carriers by

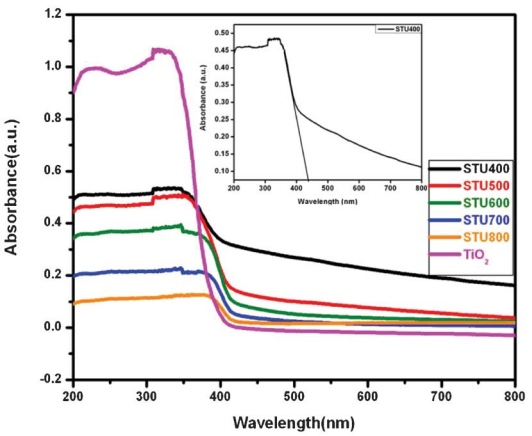

Fig. 5 UV visible absorption spectra of STU nanocomposites.

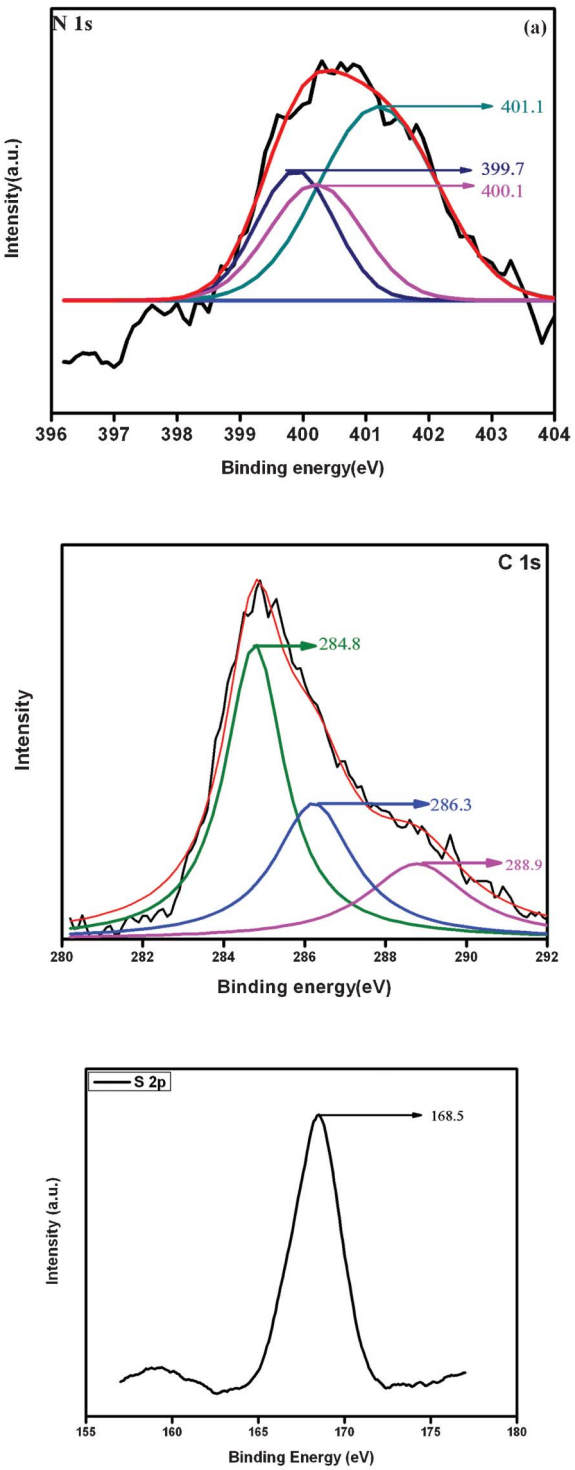

Fig. 6 (a) XPS spectra of core level N 1s (b) XPS spectra of core level C 1s (C) XPS spectra of core level S 2p.

taking photogenerated electrons.[18,19,47] Here, carbon in the N–TiO_2@CS operates as a surface sensitizer to absorb visible light and make a junction to separate the charge carrier. The atomic content of C was calculated from XPS and found to be 19.4 atom%.

Fig. 6(c) shows the S 2p core level peak around 168.5 eV and the atomic content of S was found to be 24.26 atom%. The observed peak can be attributed to the S^{+6} cation of sulfate and exists as bidentate sulfate ions on the TiO_2 surface.[30] This is consistent with the obtained FTIR peaks. It should be noted that the peaks characteristic of Ti–S bonds (162–163 eV) were not present in the S 2p spectra.[48]

Fig. S1, ESI† represents the Ti 2p XPS spectra of STU400. It is well known that Ti $2p_{3/2}$ of pure titania appears at 459 eV.[8] Here two peaks are observed at 458.4 and at 464.3 eV, assigned to Ti $2p_{3/2}$ and Ti $2p_{1/2}$ and the atomic content of Ti is found to be 20.36 atom%. In comparison with pure titania (Ti $2p_{3/2}$), the slight shifting of Ti $2p_{3/2}$ suggests that the parent Ti^{4+} are partially reduced due to incorporation of nitrogen in the TiO_2 lattice which changes the electron density distribution around the Ti.[49] The O 1s peak in the XPS spectrum shown in Fig. S2, ESI† represents two peaks centered at 529.8 and at 531.3 eV corresponding to oxygen in the TiO_2 and surface hydroxyl group, respectively.[50,51] The atomic content of O was found to be 34.2 atom%. The presence of the surface hydroxyl group takes an important role in the photocatalytic reaction because photo induced holes react with surface hydroxyl groups and yield surface bound OH radical with high oxidation capabilities.

4 Phenol degradation

To evaluate the photocatalytic activity of all the as prepared N–TiO_2@CS nanocomposites (STU), phenol degradation was carried out under direct sunlight because it is photostable and cannot be photodegraded in the absence of any photocatalyst under light irradiation. Fig. 7 represents photocatalytic degradation of phenol over STU nanocomposites, Degussa P25, UT400 and ST400. Dark adsorption experiments were performed on all the catalysts for 1 h. About 10% adsorption took place for the sample STU400. From the experimental study, it is observed that STU400 shows higher photocatalytical

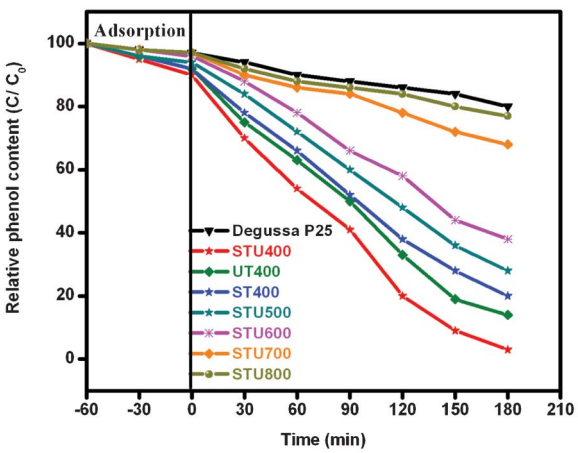

Fig. 7 Photocatalytic degradation of phenol over STU nanocomposites, UT400, ST400 and Degussa P25. C = Concentration, C_0 = Initial concentration.

activity and the degradation trend is STU400 > UT400 > ST400 > STU500 > STU600 > STU700 > STU800 > Degussa P25. The enhanced photocatalytic activity observed for the sample STU400 confirms the optimum calcined temperature is 400 °C. All the experiments were carried out under natural pH and monitored for the most active photocatalyst. The pH of the solution was measured before irradiation of light and it was found to be 5.6. During the light irradiation, the pH value decreased to 4.5 and again after 180 min it reverts back to 5.3. During the photocatalytic process, decrease in pH suggests the formation of acidic products derived from the degradation of phenol and a rise in pH after experiment is due to mineralization of phenol.

The enhanced photocatalytic activity for STU400 is attributed for several factors discussed as follows. The smaller particle size with high crystallinity anatase phase enhances diffusion of charge carriers towards the surface and rapidly reacts with adsorbed reactant. Moreover, catalytic activity is greatly influenced through smaller crystallite size.[52] As STU400 shows 100% anatase phase and small crystallite size; it might be one of the possible factors towards higher photocatalytic activity. Another most crucial factor towards enhanced visible light photocatalysis is the surface area and porosity of the catalyst.[53] High surface area coupled with wormhole mesoporous structure enhances more adsorption of the reactant molecules and the presence of wormhole architecture decreases the diffusion length of charge carriers towards the active sites and increases the rate of degradation.[8] Besides this, band gap narrowing by N doping, carbon sensitization, and electron-hole separation mediated by the C and S species are the major key factors for the enhancement in visible light photocatalytic efficiency. The lowering in photocatalytic activity observed at higher calcination temperatures (*i.e.* above 400 °C) is due to losses of N, C and S content from the N–TiO_2@CS nanocomposite and destruction of the mesoporous morphology.[54,55]

A probable visible light photocatalytic mechanism over N–TiO_2@CS nanocomposites is well explained on the basis of our observed experimental data. In the present study, incorporation of N modifies the electronic band structure of TiO_2. It leads to the formation of a localized N 2p state just above the O 2p valence band and shifts the optical absorbance towards the visible region.[14] N doping to the crystal lattice of TiO_2 (N–Ti–O) converts some of the Ti^{4+} to $Ti^{3+}$and acts as an effective main catalyst contributing towards the visible light absorption. In our system, sulfate is present as N–Ti–O–S on the catalyst surface. It exists as an S^{6+} cation in the form of adsorbed SO_4^{2-}. The surface adsorbed SO_4^{2-} enhances the surface acidity and induced Brønsted and Lewis acidic sites on the TiO_2 surface. These acidic sites may provide more chemisorption centers for reactant sites and oxygen molecules, moreover it also accepts electrons and behaves as a co-catalyst.[56,30] The presence of co-catalyst on the catalyst surface acts as an antenna which collects the photo induced charge carriers formed at the Fermi level equilibration after the light excitation and inhibits the electron-hole recombination.[30]

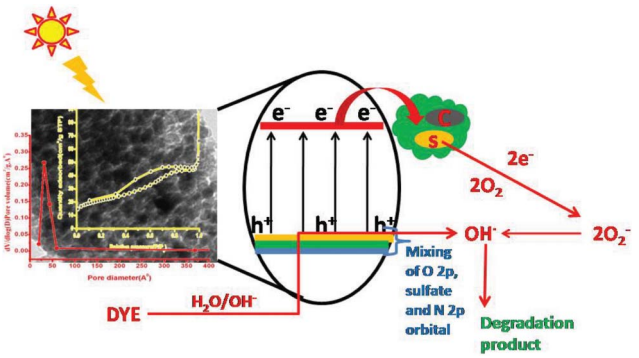

Scheme 1 The proposed photocatalytic mechanism over the N–TiO_2@CS nanocomposites.

The S^{6+} cation on the surface of the TiO_2 influences the trapping of photo excited electrons from the conduction band and reduces the system from S^{6+} to S^{4+}, because the state of S^{6+} could easily get electrons and change into S^{4+} states in the photo-catalytic process.[57,30] Furthermore, the transformation of an electron towards the surface adsorbed oxygen species produces a superoxide radical, followed by the formation of hydrogen peroxide as an intermediate product and subsequently decomposes to hydroxyl radical. This transformation of the electron again makes the system as S^{+6}; here the sulfate species undergoes a redox cycle. This type of favorable structure created by sulfate (Ti–O–S) enhances the separation of charge carriers and improves the photocatalytic activity.[30] In contrast to the above factor; another factor plays a pivotal role in our system. That is the surface adsorbed carbon species on the catalyst surface which enhances visible light absorption and reduces the reflection of light as it acts as a sensitizer. In addition to the sensitizing ability, it leads a major role to reduce recombination of charge carriers by taking the photogenerated electron from the conduction band and keep them more reactive.[18,19,58] The reactive holes react with the OH^- to form the most reactive oxygen species, $OH^{\bullet}$. Considering the above facts, a synergistic hetero structure is proposed for N–TiO_2@CS in Scheme 1, where the electron from the conduction band is transferred to a joint charge transfer transition state which is located more at the carbon. In this type of conditions, surface adsorbed water converts to a hydroxyl radical which is responsible for photo degradation. In our system, the synergistic effect of visible light absorption, faster diffusion of charge carriers due to the wormhole mesoporous frame and separation of charge carriers due to the presence of surface carbon and sulfate species gives it more potential towards visible light photocatalysis.

4.1 Analysis of $^{\bullet}OH$ radical

To confirm the above mechanism, analysis for hydroxyl radical formation was performed by using terephthalic acid. Basically, $^{\bullet}OH$ are generated from the oxidative reaction between photo generated holes and H_2O or OH^- whereas a reductive reaction takes place between photo induced electrons, O_2 and H^+.[59–61] It is known that $^{\bullet}OH$ reacts with terephthalic acid (TA) in basic

solution to generate 2-hydroxy terephthalic acid (TAOH) and emits a unique fluorescence signal with its peak centered at *ca.* 426 nm.[62] Usually, the production of the hydroxyl radical is proportional to the observed PL intensity. As shown from Fig. 8, a more intense peak centered at 426 nm was observed for STU400, but as the calcined temperature increases it shows a lower intensity peak, suggesting the formation of fewer hydroxyl radicals, confirming higher photocatalytic activity for the former. This experiment also confirms that hydroxyl radicals are the active species for the photocatalytic degradation of phenol over STU type of catalysts.

4.2 Photoluminescence (PL)

To determine the electron-hole recombination characteristics and to further confirm the mechanism, PL studies have been undertaken. It is well known that PL emission is the result of the recombination of excited electrons and holes; the lower PL intensity indicates the low recombination of electrons and holes.[63] The PL spectra is closely associated to the recombination of photo induced electron and holes, free excitation and self trapped excitations which result from surface defects in the TiO_2 crystals such as lattice distortion and surface oxygen vacancies.[64] Fig. 9 shows the PL spectra of pure TiO_2, STU400 and STU500 nanocomposites at about 393, 420, 450, 485 nm. Both the pure and N–TiO_2@CS (STU) photocatalysts show obvious PL signals with similar curves. The two peaks appeared at 393 and 420 nm might be due to self trapped excitation delocalized on TiO_6 octahedra.[65] The peak observed in the region of 450 nm is possibly the result of binding exactions.[65] Another single peak observed at 484 nm is attributed to oxygen vacancies.[66] Among all the catalysts, STU400 shows a lower PL intensity, suggesting a lower recombination rate and leading to higher photocatalytic activity.

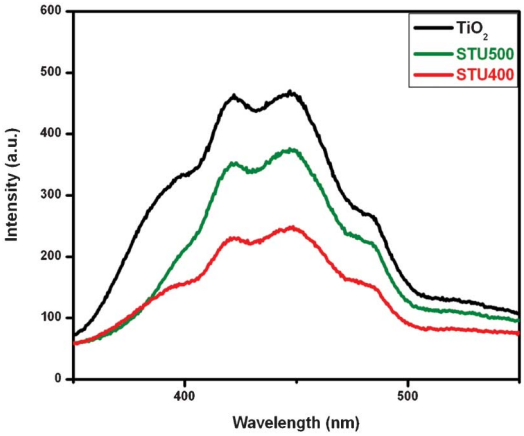

Fig. 9 Photoluminescence (PL) spectra of STU400, STU500 andTiO_2.

Conclusions

Mesoporous N–TiO_2@CS nanocomposites have been prepared by a sol–gel auto-combustion method and thoroughly characterized through various structural, textural and microscopic methods. The as-prepared N–TiO_2@CS nanocomposite calcined at 400 °C showed excellent performance for phenol degradation under visible light irradiation. In our system nitrogen exists as (N–Ti–O) which plays an essential role towards visible light absorption. Sulfate species on the catalyst surface act as a co-catalyst and contribute to the separation and transfer of charge carriers. Furthermore, the presence of surface carbon species acts as a surface sensitizer and creates a hetero structural medium for the transportation of electrons, which contributes towards higher photocatalytic activity. Not only these above factors make our system ideal but also other aspects, such as visible light absorption, high crystallinity, small crystallite size, anatase phase and high surface area with wormhole mesoporous frame, contribute to the overall increase in photocatalytic activity.

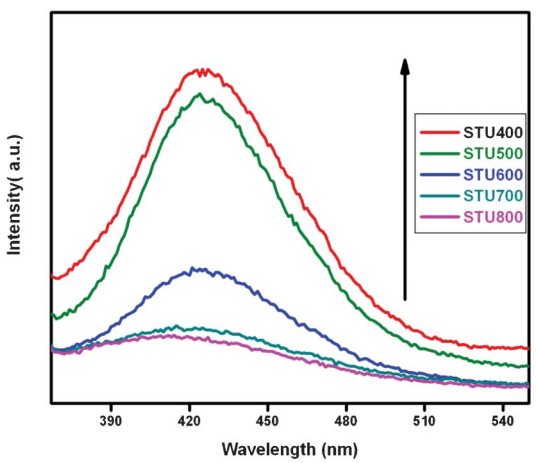

Fig. 8 •OH trapping photoluminescence (PL) spectra for STU nanocomposites.

Acknowledgements

The authors are very much thankful to Prof. B. K. Mishra, Director, IMMT, for giving permission to publish the work, Dr K. R. Patil, NCL pune, for doing XPS analyses. The financial assistance from MLP-18 greatly acknowledged.

References

1 W. H. Chiu, K. M. Lee and W. F. Hsieh, *J. Power Sources*, 2011, **196**, 3683.
2 Y. Zhang, Z. R. Tang, X. Fu and Y. Xu, *ACS Nano*, 2010, **4**, 7303.
3 S. Perera and K. Balkus Jr., *Mater. Res. Soc. Symp. Proc.*, 2010, **1211**, 115.
4 H. Yu, H. Irie, Y. Shimodaira, Y. Hosogi, Y. Kuroda, M. Miyauchi and K. Hashimoto, *J. Phys. Chem. C*, 2010, **114**, 16481.
5 X. Wang, M. Blackford, K. Prince and R. Caruso, *ACS Appl. Mater. Interfaces*, 2012, **4**, 476.

6 S. D. Mo and W. Y. Ching, *Phys. Rev. B: Condens. Matter*, 1995, **51**, 13023.
7 M. Anpo and M. Takeuchi, *J. Catal.*, 2003, **216**, 505.
8 K. Sivaranjani and C. Gopinath, *J. Mater. Chem.*, 2011, **21**, 2639.
9 P. Xu, J. Lu, T. Xu, S. Gao, B. Huang and Y. Dai, *J. Phys. Chem. C*, 2010, **114**, 9510.
10 G. Yang, Z. Yan and T. Xiao, *Appl. Surf. Sci.*, 2012, **258**, 4016.
11 S. K. Samatray and K. M. Parida, *J. Mol. Catal.*, 2001, **176**, 156.
12 K. Yang, Y. Dai and B. Huang, *J. Phys. Chem. C*, 2010, **114**, 19830.
13 G. Wu, J. Wang, D. Thomas and A. Chen, *Langmuir*, 2008, **24**, 3503.
14 R. Asahi, T. Morikawa, T. Ohwaki, K. Aoki and Y. Taga, *Science*, 2001, **293**, 269.
15 S. Livraghi, A. M. Czoska, E. Giamello and M. Paganini, *J. Solid State Chem.*, 2009, **182**, 160.
16 M. Sathish, B. Viswanathan, R. P. Viswanath and C. S. Gopinath, *Chem. Mater.*, 2005, **17**, 6349.
17 P. Zabek, J. Eberl and H. Kisch, *Photochem. Photobiol. Sci.*, 2009, **8**, 264.
18 L. Zhao, X. F. Chen, X. C. Wang, Y. J. Zhang, W. Wei, Y. H. Sun, M. Antonietti and M. M. Titirici, *Adv. Mater.*, 2010, **22**, 3317.
19 D. Wang, L. Jia, X. Wu, L. Lu and A. Xu, *Nanoscale*, 2012, **4**, 576.
20 T. Umebayashi, T. Yamaki, S. Tanaka and K. Asai, *Chem. Lett.*, 2003, **32**, 330.
21 K. Takeshita, A. Yamakata, T. Ishibashi, H. Onishi, K. Nishijima and T. Ohno, *J. Photochem. Photobiol., A*, 2006, **177**, 269.
22 T. Ohno, T. Mitsui and M. Matsumura, *Chem. Lett.*, 2003, **32**, 364.
23 S.K. Samatray, P. Mohapatra and K. M. Parida, *J. Mol. Catal. A: Chem.*, 2003, **198**, 277.
24 P. Mohapatra, S. Samantaray and K. M. Parida, *J. Photochem. Photobiol., A*, 2005, **170**, 189.
25 P. Mohapatra and K. M. Parida, *J. Mol. Catal. A: Chem.*, 2006, **258**, 118.
26 K. M. Parida, N. Sahu, N. R. Biswal, B. Naik and A. C. Pradhan, *J. Colloid Interface Sci.*, 2008, **318**, 231.
27 O. Teruhisa, M. Zenta, N. Kazumoto, K. Hidekazu and X. Feng, *Appl. Catal., A*, 2006, **302**, 62.
28 Y. Cong, F. Chen, J. Zhang and M. Anpo, *Chem. Lett.*, 2006, **35**, 800.
29 D. Chen, Z. Jiang, J. Geng, Q. Wang and D. Yang, *Ind. Eng. Chem. Res.*, 2007, **46**, 2741.
30 B. Naik, K. M. Parida and C. S. Gopinath, *J. Phys. Chem. C*, 2010, **114**, 19473.
31 N. Yao, C. Wu, L. Jia, S. Han, B. Chia, J. Pu and L. Jian, *Ceram. Int.*, 2012, **38**, 1671.
32 Q. Xiao, L. Ouyang, L. Gao and C. Yao, *Appl. Surf. Sci.*, 2011, **257**, 3652.
33 H. Sun, Y. Bai, Y. Cheng, W. Jin and N. Xu, *Ind. Eng. Chem. Res.*, 2006, **45**, 4971.
34 Q. Xiao and L. Ouyang, *J. Phys. Chem. Solids*, 2011, **72**, 39.
35 X. Bokhimi, A. Morales, E. Ortiz, T. Lopez, R. Gomez and J. Navarrete, *J. Sol-Gel Sci. Technol.*, 2004, **29**, 31.
36 P. Mohapatra, J. Moma, K. M. Parida, W. A. Jordaan and M. S. Scurrell, *Chem. Commun.*, 2007, 1044.
37 S. T. Martin, C. L. Morrison and M. R. Hoffmann, *J. Phys. Chem.*, 1994, **98**, 13695.
38 J. H. Pan, X.W. Zhang, A. J. Du, D. D. Sun and J. O. Leckie, *J. Am. Chem. Soc.*, 2008, **130**, 11256.
39 S. Basu, M. Mapa, C. Gopinath, M. Doble, S. Bhaduri and G. Lahiri, *J. Catal.*, 2006, **239**, 154.
40 G. Wang, B. Cheng, J. Zhang, L. X and T. Yin, *Int. J. Photoenergy*, 2012, **10**(1155).
41 J. Yang, H. Bai, X. Tan and J. Lian, *Appl. Surf. Sci.*, 2006, **253**, 1988.
42 M. Satish, B. Viswanathan, R. P. Viswanath and C. S. Gopinath, *J. Nanosci. Nanotechnol.*, 2009, **9**, 423.
43 X. Li, H. Zhang, X. Zheng, Z. Yin and L. Wei, *J. Environ. Sci.*, 2011, **23**, 1919.
44 B. Viswanathan and K. R. Krishanmurthy, *Int. J. Photoenergy*, 2012, **2012**, 269654.
45 B. Chi, L. Zhao and T. Jin, *J. Phys. Chem. C*, 2007, **111**, 6189.
46 H. B. Liu, Y. M. Wu and J. L. Zhang, *ACS Appl. Mater. Interfaces*, 2011, **3**, 1757.
47 H. Zhang, X. J. Lv, Y. M. Li, Y. Wang and J. H. Li, *ACS Nano*, 2010, **4**, 380.
48 W. Ho, J. Yu and S. Lee, *J. Solid State Chem.*, 2006, **179**, 1171.
49 J. Wang, W. Zhu, Y. Zhang and S. Liu, *J. Phys. Chem. C*, 2006, **111**, 1010.
50 N. C. Saha and H. G. Tompkins, *J. Appl. Phys.*, 1992, **72**, 3072.
51 F. Dong, Y. Sun and M. Fu, *Int. J. Photoenergy*, 2012, **2012**, 569716.
52 Z. Bian, J. Zhu, S. Wang, Y. Cao, X. Qian and H. Li, *J. Phys. Chem. C*, 2008, **112**, 6258.
53 I. Tsuji, H. Kobayashi and A. Kudo, *J. Am. Chem. Soc.*, 2004, **126**, 13406.
54 S. Martha, D. P. Das, N. Biswal and K. M. Parida, *J. Mater. Chem.*, 2012, **22**, 10695.
55 L. Lin, W. Lin, Y.X. Zhu, B. Y. Zhao, Y. C. Xie, Y. He and Y. F. Zhu, *J. Mol. Catal. A: Chem.*, 2005, **236**, 46.
56 F. Wei, L. Ni and P. Cui, *J. Hazard. Mater.*, 2008, **156**, 135.
57 H. Sun, H. Liu, J. Ma, X. Wang, B. Wang and L. Han, *J. Hazard. Mater.*, 2008, **156**, 552.
58 A. Xu, Y. Gao and H. Liu, *J. Catal.*, 2002, **207**, 151.
59 I. K. Konstantinou and T. A. Albanis, *Appl. Catal., B*, 2004, **49**, 1.
60 N. Daneshvar, D. Salari and A. R. Khataee, *J. Photochem. Photobiol., A*, 2003, **157**, 111.
61 J. Zhang, J. Xi and Z. Ji, *J. Mater. Chem.*, 2012, **22**, 17700.
62 T. Hirakawa and Y. Nosaka, *Langmuir*, 2002, **18**, 3247.
63 Y. Li, H. Zhang, Z. Guo, J. Han, X. Zhao, Q. Zhao and S. Kim, *Langmuir*, 2008, **24**, 8351.
64 L. Zhang and C. Mo, *Nanostruct. Mater.*, 1995, **6**, 831.
65 J. Zhou, Y. Zhang, X. Zhao and A. Ray, *Ind. Eng. Chem. Res.*, 2006, **45**, 3503.
66 Q. Xiao, Z. Si, Z. Yu and G. Qiu, *Mater. Sci. Eng., B*, 2007, **137**, 189.

